

ACCEPTED MANUSCRIPT • OPEN ACCESS

## Deep learning of chaos classification

To cite this article before publication: Woo Seok Lee *et al* 2020 *Mach. Learn.: Sci. Technol.* in press <https://doi.org/10.1088/2632-2153/abb6d3>

### Manuscript version: Accepted Manuscript

Accepted Manuscript is “the version of the article accepted for publication including all changes made as a result of the peer review process, and which may also include the addition to the article by IOP Publishing of a header, an article ID, a cover sheet and/or an ‘Accepted Manuscript’ watermark, but excluding any other editing, typesetting or other changes made by IOP Publishing and/or its licensors”

This Accepted Manuscript is © 2020 The Author(s). Published by IOP Publishing Ltd.

As the Version of Record of this article is going to be / has been published on a gold open access basis under a CC BY 3.0 licence, this Accepted Manuscript is available for reuse under a CC BY 3.0 licence immediately.

Everyone is permitted to use all or part of the original content in this article, provided that they adhere to all the terms of the licence  
<https://creativecommons.org/licenses/by/3.0>

Although reasonable endeavours have been taken to obtain all necessary permissions from third parties to include their copyrighted content within this article, their full citation and copyright line may not be present in this Accepted Manuscript version. Before using any content from this article, please refer to the Version of Record on IOPscience once published for full citation and copyright details, as permissions may be required. All third party content is fully copyright protected and is not published on a gold open access basis under a CC BY licence, unless that is specifically stated in the figure caption in the Version of Record.

View the [article online](#) for updates and enhancements.

# Deep Learning of Chaos Classification

Woo Seok Lee<sup>1</sup> and Sergej Flach<sup>1,2</sup>

<sup>1</sup>Center for Theoretical Physics of Complex Systems, Institute for Basic Science,  
34051 Daejeon, Korea

<sup>2</sup>Basic Science Program, Korea University of Science and Technology (UST), 34113  
Daejeon, Korea

E-mail: [wooseoklee06@gmail.com](mailto:wooseoklee06@gmail.com)

July 2020

**Abstract.** We train an artificial neural network which distinguishes chaotic and regular dynamics of the two-dimensional Chirikov standard map. We use finite length trajectories and compare the performance with traditional numerical methods which need to evaluate the Lyapunov exponent. The neural network has superior performance for short periods with length down to 10 Lyapunov times on which the traditional Lyapunov exponent computation is far from converging. We show the robustness of the neural network to varying control parameters, in particular we train with one set of control parameters, and successfully test in a complementary set. Furthermore, we use the neural network to successfully test the dynamics of discrete maps in different dimensions, e.g. the one-dimensional logistic map and a three-dimensional discrete version of the Lorenz system. Our results demonstrate that a convolutional neural network can be used as an excellent chaos indicator.

## 1. Introduction

Chaotic dynamics exists in many natural systems, such as heartbeat irregularities, weather and climate [1, 2]. Such dynamics can be studied through the analysis of proper mathematical models which generate nonlinear dynamics and deterministic chaos. Chaotic and regular dynamics can co-exist in the phase space of low-dimensional systems [3]. To distinguish chaotic from regular dynamics, tangent dynamics is used to compute Lyapunov exponents  $\lambda$ . In practice one integrates the tangent dynamics along a given trajectory and averages a finite time Lyapunov exponent  $\lambda(t)$ . The averaging time  $T$  needed to reliably tell regular ( $\lambda = 0$ ) from chaotic ( $\lambda \neq 0$ ) trajectories apart is usually orders of magnitude larger than the Lyapunov time  $T_\lambda \equiv 1/\lambda$ .

Here, we introduce a machine learning approach that alleviates the problems of calculating Lyapunov exponents and can be used as a new chaos indicator. Machine learning has shown tremendous performance e.g. in pattern recognition [4, 5]. Machine learning approaches turned useful to solve partial differential equations and identify hidden physics models from experimental data [6–8]. Machine learning was used recently

1  
2     *Deep Learning of Chaos Classification*  
3  
4  
5  
6  
7  
8  
9  
10  
11  
12  
13  
14  
15  
16  
17  
18  
19  
20  
21  
22

to predict future chaotic dynamics details from time series data without knowledge of the generating equations [9, 10]. In this paper, we introduce a machine learning way to use short time series data for telling chaos from regularity apart. We train a neural network using chaotic and regular trajectories from the Chirikov standard map. Our method has a success rate of 98% using trajectories with length  $10T_\lambda$ , while conventional methods need up to  $10^4T_\lambda$  to reach the same accuracy. The main reason for the small but finite failure rate of our machine learning method is due to sticky orbits. These orbits are chaotic, yet can mimic regular ones for long times due to trapping in fractal boundary phase space regions separating chaotic and regular dynamics. Our method is also surprisingly successful when trained with Standard Map data but tested on maps with different dimensions such as the logistic map ( $d = 1$ ) and the Lorenz system ( $d = 3$ ).

20  
21     **2. The Chirikov Standard Map**  
22  
23  
24  
25

The Chirikov standard map is an area-preserving map in dimension  $d = 2$  [11] also known as the kicked rotor [3]

$$\begin{aligned} p_{n+1} &= p_n + \frac{K}{2\pi} \sin(2\pi x_n) \quad \text{mod } 1, \\ x_{n+1} &= x_n + p_{n+1} \quad \text{mod } 1. \end{aligned} \quad (1)$$

The kick strength  $K$  controls the degree of nonintegrability and chaos appearing in the dynamics generated by the map.

Consider the case when  $K = 0$ . Eq. 1 reduces to  $p_{n+1} = p_n \pmod{1}$  and  $x_{n+1} = x_n + p_{n+1} \pmod{1}$  which is integrable and every orbit resides on an invariant torus. The orbit can exhibit periodic or quasi-periodic behavior depending on the initial conditions  $(p_0, x_0)$ . For small values of  $K$  e.g.  $K = 0.5$  (Fig.1(a)) most of these orbits persist, with tiny regions of chaotic dynamics appearing which are not visible on the presented plotting scales. At  $K = K_c \approx 0.97$  the last invariant KAM tori are destroyed and a simply connected chaotic sea is formed which allows for unbounded momentum diffusion. For larger values of  $K$  the chaotic fraction grows confining regular dynamics to regular islands embedded in a chaotic sea (Fig. 1). Further increase of  $K$  leads to a flooding of the regular islands by the chaotic sea.

47  
48     **3. Lyapunov exponents and predictions**  
49  
50  
51  
52

The Lyapunov exponent (LE) characterizes the exponential rate of separation of a trajectory  $\{p_n, x_n\}$  and its infinitesimal perturbation  $\{\delta_n, \zeta_n\}$ :

$$\begin{aligned} p_{n+1} + \delta_{n+1} &= (p_n + \delta_n) + \frac{k}{2\pi} \sin(2\pi(x_n + \zeta_n)) \\ x_{n+1} + \zeta_{n+1} &= (x_n + \zeta_n) + (p_{n+1} + \delta_{n+1}) \end{aligned} \quad (2)$$

Linearizing (2) in the perturbation yields the tangent dynamics generated by the variational equations

53  
54  
55  
56  
57  
58  
59  
60

## Deep Learning of Chaos Classification

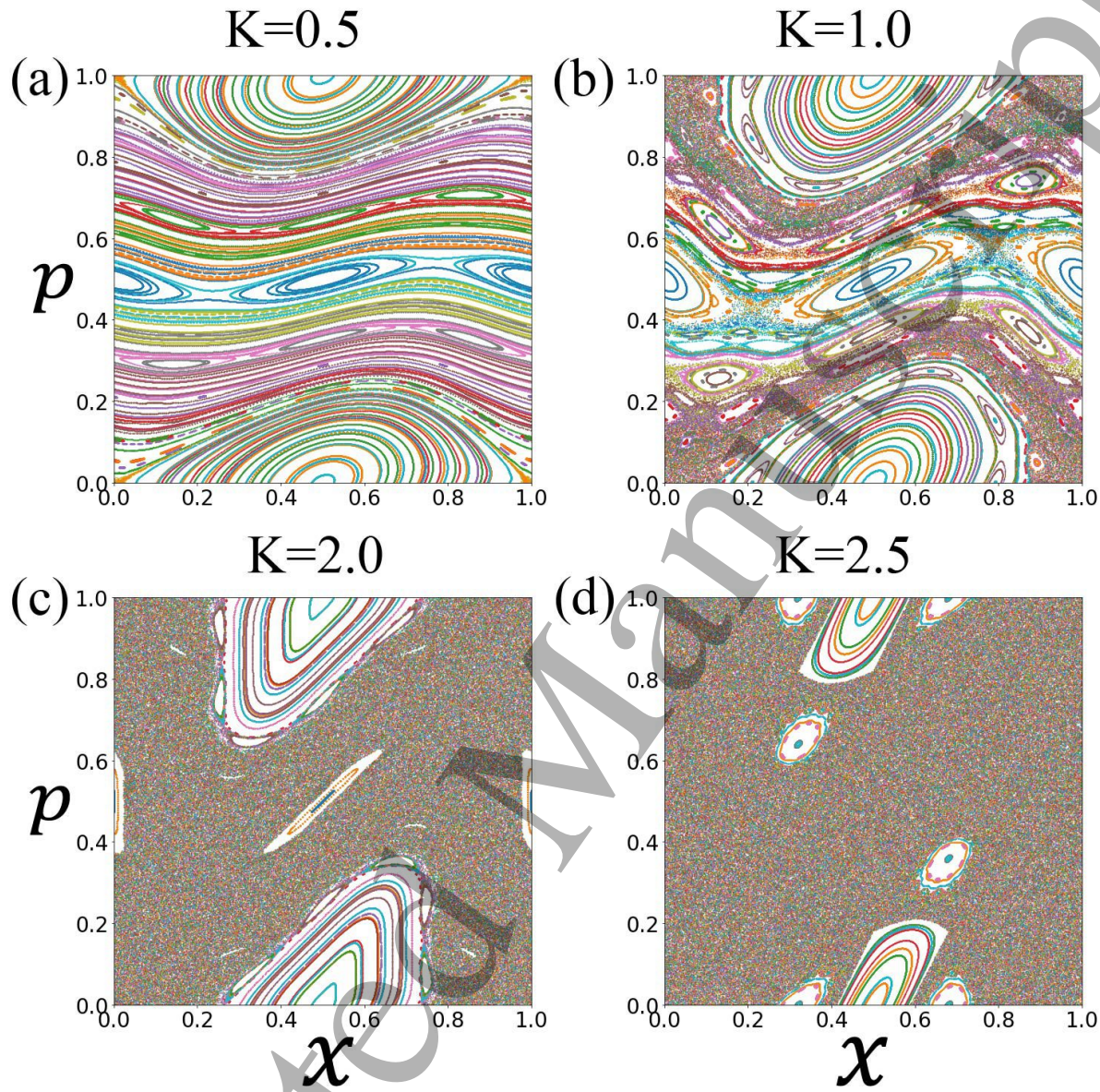


**Figure 1.** Examples of phase portraits (Poincaré sections) of the standard map. (a)  $K=0.5$ , (b)  $K=1.0$ , (c)  $K=2.0$ , (d)  $K=2.5$ .

$$\begin{aligned}\delta_{n+1} &= \delta_n + k\zeta_n \cos(2\pi x_n) \\ \zeta_{n+1} &= \zeta_n + \delta_{n+1}\end{aligned}\tag{3}$$

For computational purposes  $\delta$  and  $\zeta$  can be rescaled after any time step without loss of generality, while keeping the rescaling factor. The LE  $\lambda$  for each trajectory is obtained from the time dependence of  $\lambda_N$ :

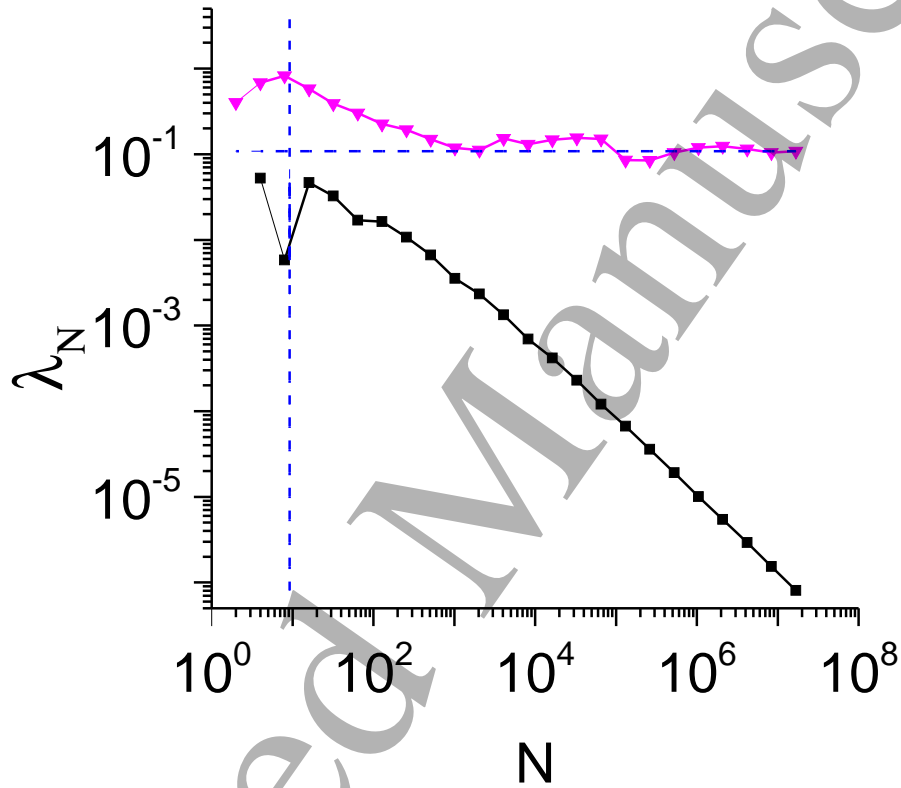
$$\lambda_N = \frac{1}{N} \sum_{n=2}^N \ln\left(\frac{\sqrt{\delta_n^2 + \zeta_n^2}}{\sqrt{\delta_{n-1}^2 + \zeta_{n-1}^2}}\right), \quad \lambda = \lim_{N \rightarrow \infty} \lambda_N.\tag{4}$$

The Lyapunov time is then defined as  $T_\lambda \equiv 1/\lambda$ . For the main chaotic sea it

1  
2     *Deep Learning of Chaos Classification*  
3  
4

5     is a function of the control parameter  $K$ . A suitable fitting function yields  $\lambda \approx$   
6      $\ln(0.7 + 0.42K)$  [12].

7     For a regular trajectory  $\lambda_N \sim 1/N$  and  $\lambda = 0$ , at variance to a chaotic trajectory  
8     for which  $\lambda_N$  saturates at  $\lambda$  at a time  $N \approx T_\lambda$ . Technically this saturation, and the value  
9     of  $\lambda$  can be safely confirmed and read off only on time scales  $N \approx 10^2..10^3 T_\lambda$ , without  
10    becoming a quantifiable distinguisher of the two types of trajectories, see Fig.2.  
11  
12



41     **Figure 2.**  $\lambda_N$  versus  $N$  for a chaotic (triangles) respectively regular (squares)  
42     trajectory with  $K = 1.0$ . The dashed horizontal line indicates the value of  $\lambda$  for  
43     the chaotic trajectory, and the dashed vertical one the corresponding value of  $T_\lambda$ .

44  
45     To quantify our statements, we run the standard map at  $K = 2.5$  Fig.1(d). We  
46     use a grid of  $51 \times 51$  points which partitions the phase space  $\{p, x\}$  into a square  
47     lattice. We use the corresponding 2601 initial conditions and generate trajectories.  
48     Each trajectory returns a function  $\lambda_N$ . We plot the resulting histogram for  $N = 20$   
49     and  $N = 3 \cdot 10^5$  in Fig.3 (a) and (b) respectively. For  $N \rightarrow \infty$  the histogram should  
50     show two bars only - one at  $\lambda_N = 0$  (all regular trajectories) and one at  $\lambda_N = \lambda$  (all  
51     chaotic trajectories). For finite  $N$  the distributions smoothen. Note that even negative  
52     values  $\lambda_N$  are generated due to fluctuations and finite averaging times. To tell chaotic  
53     from regular dynamics apart, we use the following protocol. We identify the two largest  
54     peaks in each histogram, and identify the threshold dividing dynamics into regular and  
55     chaotic as the deepest minimum between them (in case of a degeneracy, the one with the  
56     57  
58  
59  
60

### Deep Learning of Chaos Classification

smallest value of  $\lambda_N$ ). The location of the threshold is shown for  $N = 20$  and  $N = 3 \cdot 10^5$  in Fig.3 (a) and (b) respectively. We then assign a chaos respectively regular label to each trajectory. This label can fluctuate as a function of time for any given trajectory. We use the division for the largest simulation time  $N = 3 \cdot 10^5$  as a reference ('true') label for all trajectories. The success rate in predicting the correct regular  $P_R$  or chaotic  $P_C$  label is defined by the ratio of the correctly predicted labels within each subgroup of identical true labels. Likewise the success rate of predicting any label correctly is denoted by  $P_{tot}$ . The results are plotted versus time  $N$  in Fig.3 (c). While regular labels are predicted with high accuracy, chaotic ones are reaching 98% at only  $N \approx 10^3 T_\lambda$ .

The low success rate  $P_C$  is therefore also lowering the total success rate  $P_{tot}$ .

## 4. Neural networks and predictions

The input data of an artificial neural network consisting of only fully connected layers are limited to a one-dimensional (array) form [13]. Fully connected layers connect all the inputs from one layer to every activation unit of the next layer. The standard map generates sequences embedded in two dimensions. In order to learn data embedded in dimensions two or larger, the data must be flattened, and spatial information can get lost. A Convolutional Neural Network (CNN) is known to learn while maintaining spatial informations of images [14]. A CNN is usually configured with convolution and pooling layers. The former employ convolutional integrals with input data and filters to produce output feature maps. An additional activation function turns the network non-linear. At the end of the convolution layers a pooling layer is added which performs value extraction in a given pooling region. Through multiple convolution layers and pooling layers, the network can improve its prediction features.

Finally, a fully connected layer generates classified output data. For binary classification, the last layer consists of one node. Its output value is either zero or one. We refer the reader to Appendix A for further technical details of the CNN we use.

### 4.1. The standard map

The input of the neural network is a time series  $(p_n, x_n)$  from Eq. 1. The trajectory  $(p_n, x_n)$  shows regular or chaotic behavior depending on the initial values  $(p_0, x_0)$ . Each of the trajectories is assigned a class label based on the Lyapunov time: Class  $R$  corresponds to a non-chaotic trajectories while  $C$  corresponds to a chaotic trajectories. We remind that the phase space is discretized into  $51 \times 51 = 2601$  grid points. The training and testing is quantified with a set of parameters: i)  $K_{min}$  and  $K_{max}$  denote the range of training values of  $K$  on an equidistant grid with  $M_K$  values; ii)  $M_{tr}$  is the number of training trajectories per  $K$  value; iii)  $N_K$  is the training trajectory length; iv)  $M_{tt}$  is the number of test trajectories per  $K$  value.

To quantify the CNN performance, we assign a discrete label to each of the initial phase space points -  $C$  respectively  $R$  based on the Lyapunov exponent method with

1  
2      *Deep Learning of Chaos Classification*  
3  
4

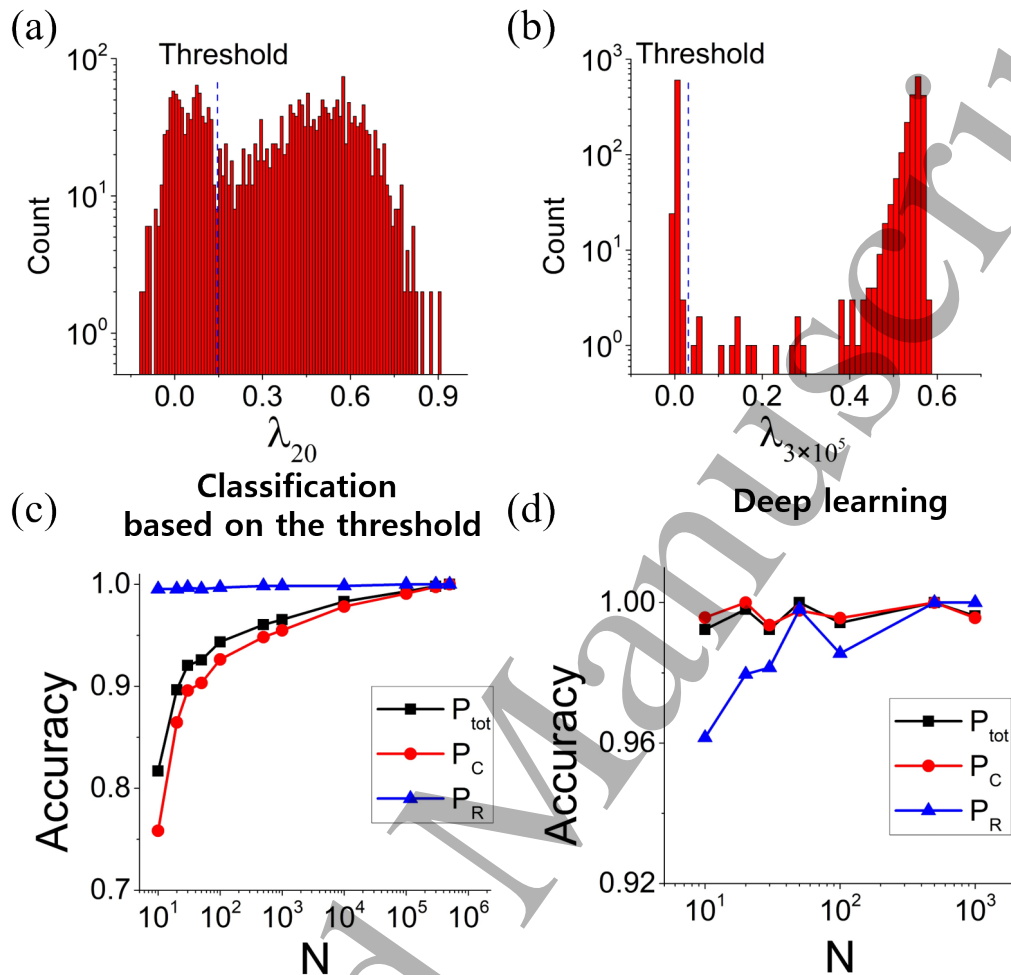


Figure 3. Performance comparison of a Lyapunov exponent based method and a deep learning method to distinguish chaotic and regular trajectories for  $K = 2.5$  and  $\lambda \approx 0.56$ . (a) Histogram of  $\lambda_{N=20}$ . the dashed vertical line indicates the location of the threshold (see text for details). (b) Same as (a) but  $N = 3 \times 10^5$ . (c) The success rates  $P_R$ ,  $P_C$  and  $P_{tot}$  as a function of  $N$  for the Lyapunov exponent based method (see text for details). (d) Same as in (c) but for the deep learning based method. The network was trained for  $K = 2.5$  and 2081 trajectories. The remaining 520 trajectories are used for testing.  $N$  in (d) represents the trajectory length used for network training and test.  $K_{min} = K_{max} = 2.5$ ,  $M_{tr} = 2081$ ,  $M_{tt} = 520$ ,  $N_K \equiv N$

trajectory length  $N = 3 \cdot 10^5$ . This way we separate all phase space points into two sets -  $C$  and  $R$ , each containing  $A_C$  and  $A_R$  points. We then run the CNN prediction on trajectories of length  $N = 20$  which start from each of the gridded phase space points. We compute the accuracy quantifying probabilities

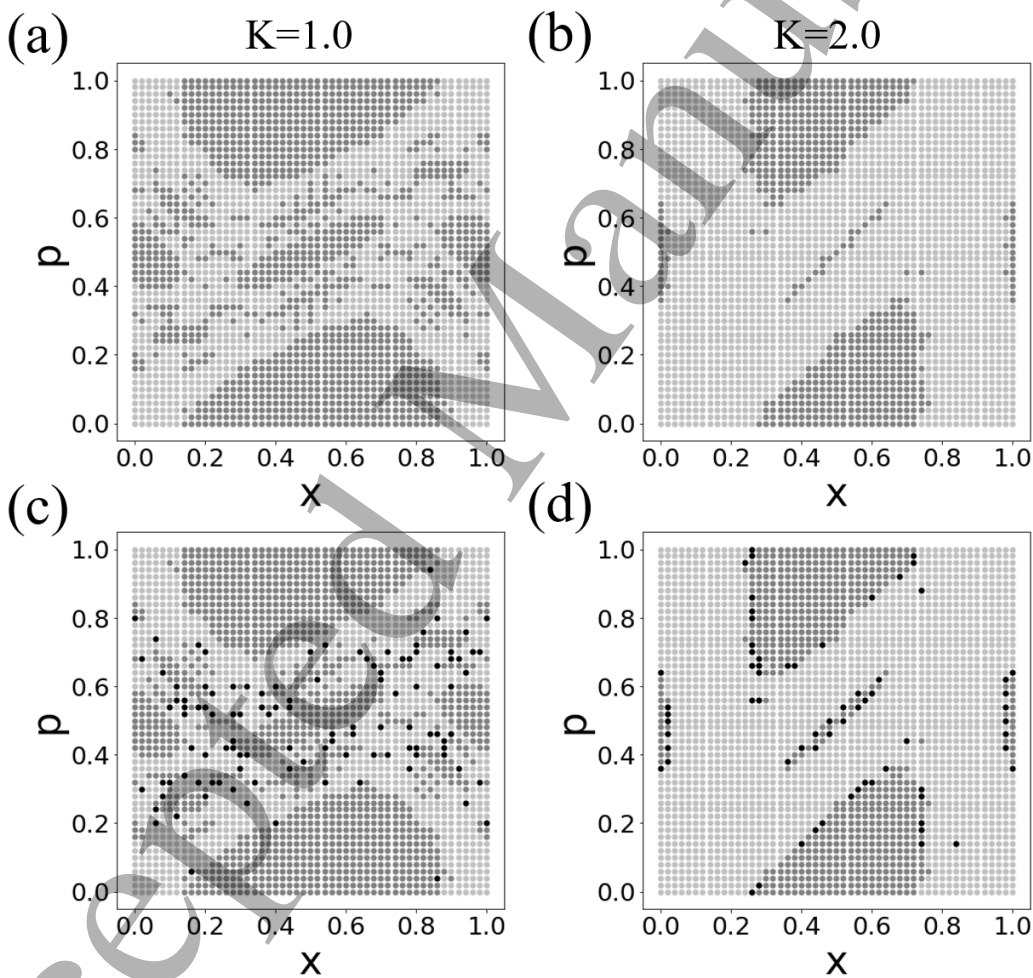
$$P_C = \frac{B_C}{A_C}, \quad P_R = \frac{B_R}{A_R}, \quad P_{tot} = \frac{B_C + B_R}{A_C + A_R} \quad (5)$$

where  $B_C$  and  $B_R$  are the numbers of trajectories predicted by the CNN to be chaotic respectively regular within each of the true sets  $A_C$  and  $A_R$ . Thus strictly

1  
2      *Deep Learning of Chaos Classification*  
3  
4  
5

6       $B_C \leq A_C$  and  $B_R \leq A_R$ .  
7

8      Fig. 3(d) compares the CNN performance to the standard Lyapunov base one.  
9      Accuracies of 98% and more are reached by the CNN for trajectory length  $N_K \geq 30$ .  
10     Similar accuracies need trajectory length  $N \approx 10^4$  and more when using standard  
11     Lyapunov testing. Fig.4 shows the CNN performance with  $N_K = 10$  in the phase  
12     space of the standard map. We observe that most of the failures correspond to  
13     chaotic trajectories starting in the fractal border region close to regular islands. These  
14     trajectories can be trapped for long times in the border region, with trapping time  
15     distributions exhibiting power law tails [15].  
16  
17



50      **Figure 4.** Chaos classification in the standard map. The Lyapunov exponent  
51      classification with trajectory length  $N = 3 \cdot 10^5$  is used as a reference classifier for  
52       $K = 1$  (a) and  $K = 2$  (b). The CNN test results are shown for  $K = 1$  (c) and  $K = 2$   
53      (d). Open circles - regular, gray circles - chaotic. Black circles show the error locations  
54      of the CNN prediction. The CNN parameters are  $K_{min} = 1.0$ ,  $K_{max} = 2.0$ ,  $M_K = 11$ ,  
55       $M_{tr} = 2081$ ,  $M_{tt} = 520$ ,  $N_K = 10$ .  
56  
57

58      To quantify the performance of the CNN, we first vary the  $N_K$  from 1 to 20  
59      (Table 1). The network is trained with chaotic and regular trajectories for  $K_{min} = 1.0$ ,  
60

1  
2     *Deep Learning of Chaos Classification*  
3  
4  
5  
6  
7  
8  
9  
10  
11  
12

$K_{max} = 2.0$ ,  $M_K = 11$ , and  $1 \leq N_K \leq 20$  and the network performance is evaluated for  $3 \leq K \leq 3.5$  and  $M_K = 6$ . The CNN requires that the length of test trajectories is always kept equal to the length of the training trajectories. Note that the Lyapunov time  $T_\lambda \approx 2$  for the test values of  $K$ . The CNN shows improvement of the accuracy with increasing  $N_K$ . While the performance fluctuates with varying  $K$ , it shows excellent results for  $N_K$  values and clearly outperforms the Lyapunov exponent based method.

K \ $N_K$	20	18	16	14	12	10	2	1
K	$P_C/P_R$							
3.0	0.99/0.99	0.93/0.98	0.95/0.98	0.92/0.98	0.97/0.96	0.83/0.95	0.89/0.97	0.78/1.0
3.1	0.90/0.98	0.94/0.96	0.96/0.96	0.93/0.96	0.90/0.96	0.83/0.91	0.90/0.93	0.79/1.0
3.2	0.93/0.95	0.94/0.97	0.96/0.97	0.93/0.97	0.97/0.94	0.85/0.91	0.90/0.92	0.79/1.0
3.3	0.97/0.99	0.93/0.99	0.95/0.99	0.93/0.99	0.94/0.96	0.85/0.93	0.89/0.98	0.77/1.0
3.4	0.94/0.99	0.89/0.97	0.94/0.96	0.92/0.98	0.93/0.97	0.82/0.93	0.88/0.98	0.76/1.0
3.5	0.93/0.94	0.93/0.93	0.96/0.88	0.92/0.99	0.92/0.91	0.83/0.92	0.87/0.94	0.76/1.0

23     **Table 1.** CNN performance. For each  $K$  value, 2601 different initial values ( $p_{0,i}, x_{0,j}$ )  
24     were selected as ( $p_{0,i} = (i-1)\frac{1}{50}, x_{0,j} = (j-1)\frac{1}{50}, (i, j \in \mathbb{Z}, 1 \leq i, j \leq 51, )$ ). Other  
25     parameters are listed in the main text.  
26

27     We then further test the CNN performance for untrained  $K$  values by varying  
28     the training  $K$  range and other relevant training parameters in Fig. 5. The network  
29     shows better performance on untrained  $K$  values when trained with a set of different  $K$   
30     values. As expected, smaller numbers of training  $K$  values yield poorer accuracy due  
31     to overtraining. With increasing training range of  $K$  values and ranges the network  
32     improves its chaos region predictions for untrained  $K$  values.  
33  
34

35     4.2. *Training with the standard map, testing the logistic map*  
36  
37

38     We proceed with testing how the CNN trained with standard map data performs in  
39     predicting chaos for other maps. We choose the logistic map as a simple one-dimensional  
40     chaotic test bed. The logistic map is written as  $x_{n+1} = rx_n(1 - x_n)$ . The parameter  $r$   
41     controls the crossover from regular to chaotic dynamics, which happens at  $r_c \approx 3.56995$ .  
42     We choose the initial condition  $x_0 = 0.4$  and iterate over 40 steps. After that we  
43     record the next 110  $x$ -values and plot them for each value of  $r$  in Fig. 6 (a,b). We  
44     observe the well-known periodic orbits, the period doubling bifurcations, and the route  
45     to chaos. The corresponding Lyapunov exponent is plotted in Fig.6(c) as a function of  $r$   
46     and shows that periodic orbits stay regular (negative Lyapunov exponent) while chaotic  
47     attractors show positive Lyapunov exponents.  
48  
49

50     We use two training methods. The first one trains the network only with the  $p_n$   
51     data sequence from the standard map in Eq. 1. We coin that trained network 1D. In that  
52     case we used a sequence of  $N_K = 20$  consecutive logistic map iteration data  $x_n, \dots, x_{n+19}$   
53     as test data.  
54  
55

56     The second training method is the original CNN one discussed above for the  
57     standard map, coined here 2D. The network input trained by the standard map has  
58  
59  
60

## Deep Learning of Chaos Classification

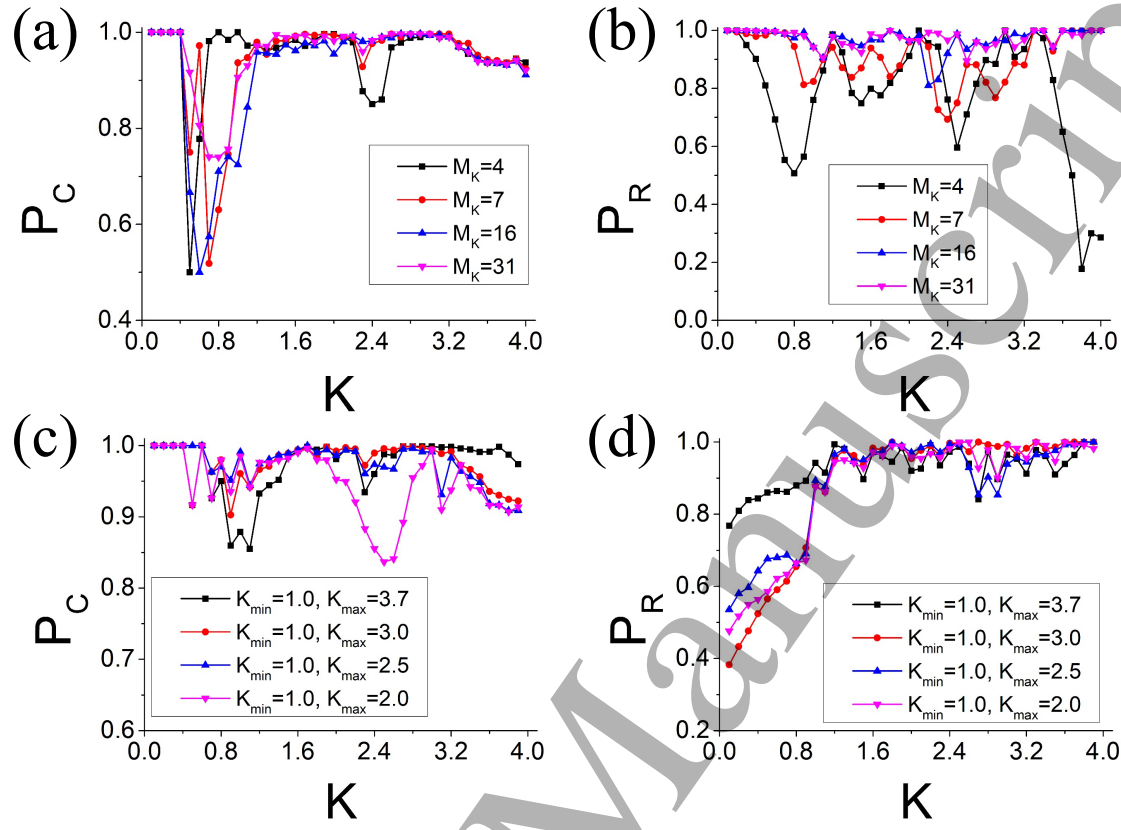


**Figure 5.** Network performance versus  $K$  for different trained  $K$  value numbers and ranges. (a), (b) Varying the number of  $K$  values used for network training in a fixed interval with equidistant spacing ( $K_{min} = 0.1$ ,  $K_{max} = 3.1$   $M_{tr} = 2081$ ,  $M_{tt} = 2601$ ,  $N_K = 20$ ). (black square)  $M_K = 4$ . (red circle)  $M_K = 7$ . (blue triangle)  $M_K = 16$ . (magenta inverted triangle)  $M_K = 31$ . (c), (d) Varying the interval of trained  $K$  values. The range of  $K$  values used in network learning are (black square)  $K_{min} = 1.0$ ,  $K_{max} = 3.7$ ,  $M_K = 28$ , (red circle)  $K_{min} = 1.0$ ,  $K_{max} = 3.0$ ,  $M_K = 21$ , (blue triangle)  $K_{min} = 1.0$ ,  $K_{max} = 2.5$ ,  $M_K = 16$ , (magenta inverted triangle)  $K_{min} = 1.0$ ,  $K_{max} = 2.0$ ,  $M_K = 11$ . The length of the input trajectories are 20.

the shape of an array with two columns each of length  $N_K = 20$  (see Appendix A). We write  $N_K = 20$  consecutive logistic map iteration data into the first column, and the next  $N_K = 20$  ones into the second column to obtain a test input vector.

As shown in Fig. 6, the network mainly generates errors at the boundary between the chaos and regular regions similar to the standard map. For  $2.5 \leq r \leq 4.0$  the accuracy is 84% for 2D network and 90% for the 1D network.

1  
2     *Deep Learning of Chaos Classification*  
3  
4  
5  
6  
7  
8  
9  
10  
11  
12  
13  
14  
15  
16  
17  
18  
19  
20  
21  
22  
23  
24  
25  
26  
27  
28  
29  
30  
31  
32  
33  
34  
35  
36  
37  
38  
39  
40  
41  
42  
43  
44  
45  
46  
47  
48  
49  
50  
51  
52  
53  
54  
55  
56  
57  
58  
59  
60

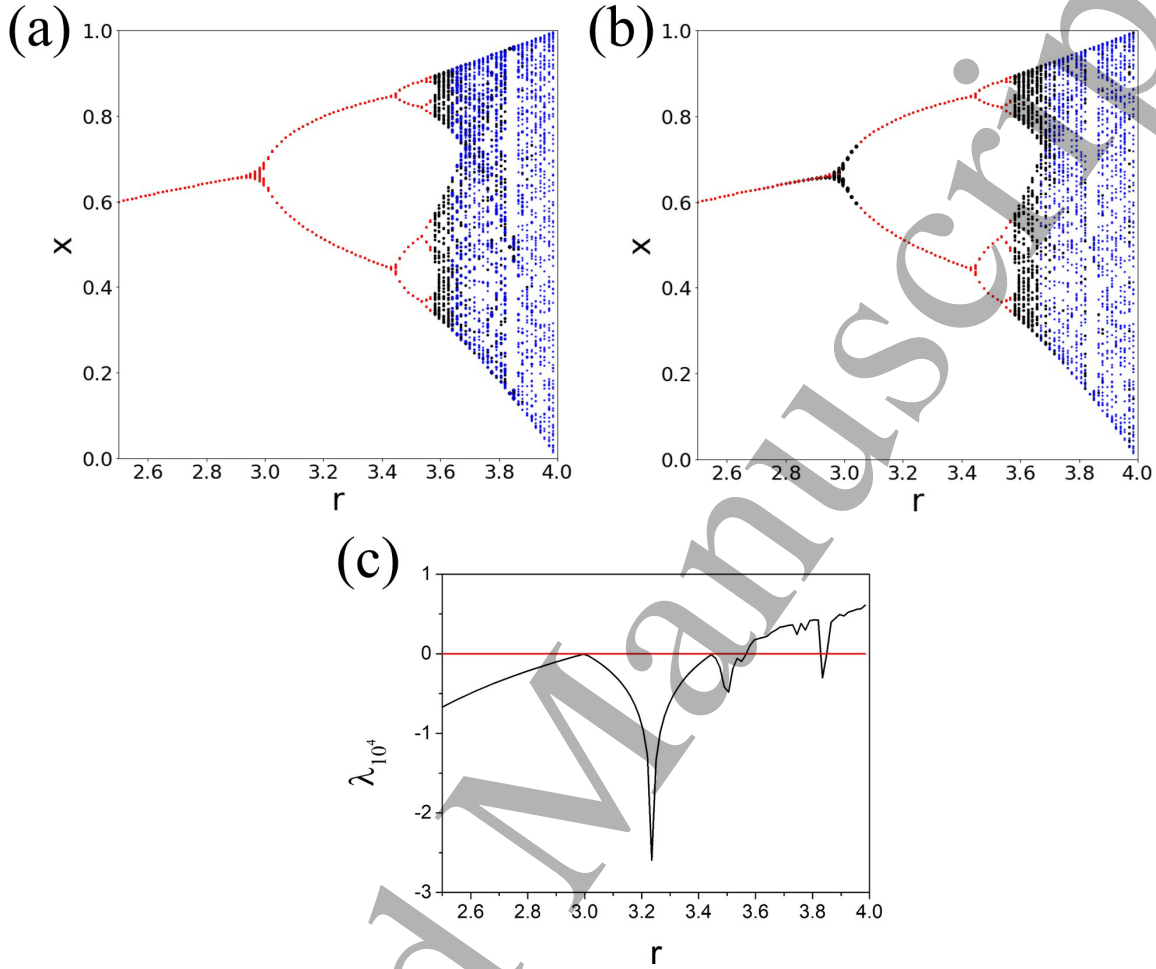


**Figure 6.** The result of predictions for the logistic map with a network trained from the standard map. The blue and red dots in bifurcation diagram are the cases where the network correctly predicts chaotic and regular attractors respectively. The black dots show where the prediction fails. The network is trained with  $K_{min} = 1.0$ ,  $K_{max} = 2.0$ ,  $M_K = 11$ ,  $M_{tr} = 2081$ ,  $M_{tt} = 520$ , and  $N_K = 20$ . (a) Test results for the 2D training (see text for details). (b) Test results for the 1D training (see text for details). (c) Lyapunov exponents for the logistic map. The red line marks  $\lambda = 0$ .

#### 4.3. Training with the standard map, testing the Lorenz system

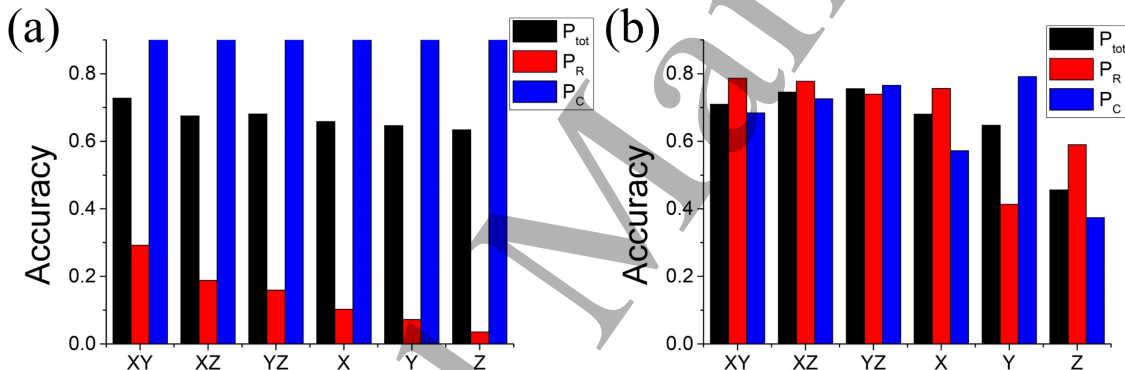
Next we test the Lorenz system - a set of three coupled nonlinear ordinary differential equations. We discretize time to arrive at a three-dimensional map:

$$\begin{aligned} X_{n+1} &= X_n + \sigma \Delta(Y_n - X_n), \\ Y_{n+1} &= Y_n + \rho \Delta X_n - \Delta X_n Z_n - \Delta Z_n, \\ Z_{n+1} &= Z_n + \Delta X_n Y_n - \beta \Delta Z_n. \end{aligned} \quad (6)$$

We use a CNN trained on the two-dimensional standard map. The parameters  $\sigma = 10$  and  $\beta = \frac{8}{3}$ . The time step  $\Delta = 0.001$  measures the discretized time interval length when replacing the original differential equations with a map.

1  
2     *Deep Learning of Chaos Classification*     11  
3  
4  
5  
6  
7  
8  
9  
10  
11  
12  
13  
14  
15  
16  
17  
18  
19  
20  
21

The chaos parameter  $0 \leq \rho \leq 39.8$  was varied in steps of 0.2. Because the network is trained with 2D data (standard map), the prediction is performed by selecting only two dimensions in the 3D Lorenz system ( $(X_n, Y_n)$ ,  $(X_n, Z_n)$ ,  $(Y_n, Z_n)$ ). As Fig. 7 (a) shows, using trajectories obtained from Eq. 6 directly as a network input classifies most of them as chaotic. We think this happens because the trajectory data of the standard map used for training are bounded between 0 and 1, but the trajectories from Lorenz system are not. Input values that exceed these boundaries cause nodes in the network to be active regardless of the input characteristics. Therefore we normalize the input data from the Lorenz system. This leads to a drastic increase of accuracy as shown in Fig. 7 (b). We also tested the outcome when selecting only one dimension in the Lorenz system for the input vector. We find a strong reduction of the accuracy. We therefore conclude that the training and testing data are yielding best performance when for both the minimum of the two dimensions (training map, testing map) is chosen.



37     **Figure 7.** The result of predictions for the Lorenz system with a network trained  
38     from the standard map. The XY, XZ, YZ bars represent the dimensions of the Lorenz  
39     system used as input to the network trained with  $(p, x)$  data from the standard map.  
40     The training conditions are  $N_K = 20$ ,  $K_{min} = 1.0$ ,  $K_{max} = 2.0$ , and  $M_K = 11$ . The  
41     X, Y, Z bars represent the single dimensions of the Lorenz system used as input to  
42     the network trained with  $p$  data only from the standard map. (a) Accuracy without  
43     normalizing the trajectories of the Lorenz system. (b) Accuracy when normalizing  
44     trajectories of the Lorenz system.  
45  
46  
47

## 48     5. Conclusion

We trained convolutional neural networks with time series data from the two-dimensional standard map. As a result, the network can classify unknown short trajectory sequences into chaotic or regular with high accuracy. To reach accuracies of up to 98% we need trajectory segments with length less than 5-10 Lyapunov times. Similar accuracies need 100-1000 longer segments when using traditional classifiers based on measuring Lyapunov exponents. The main cause of errors is due to fractal phase space structures at the boundaries between chaotic and regular dynamics. Trajectories launched in these

1  
2     *Deep Learning of Chaos Classification*     12  
3  
4  
5  
6  
7  
8  
9  
10  
11  
12  
13  
14  
15  
16  
17  
18  
19  
20  
21  
22  
23  
24  
25  
26  
27  
28  
29  
30  
31  
32  
33  
34  
35  
36  
37  
38  
39  
40  
41  
42  
43  
44  
45  
46  
47  
48  
49  
50  
51  
52  
53  
54  
55  
56  
57  
58  
59  
60

regions yield sticky trajectories which can mimic regular ones for long times, only to escape at even larger times into the chaotic sea. We also used a network trained with two-dimensional standard map data to classify chaotic and regular dynamics in one- and three-dimensional maps. Surprisingly high accuracy is reached when the training data are projected into one dimension for predictions on the one-dimensional logistic map, and when to-be-predicted data from the three-dimensional Lorenz system are projected onto two dimensions. We conclude that accuracy is optimized when the minimum of the two dimensions (training map, testing map) is chosen for both training and testing.

### Acknowledgments

This work was supported by the Institute for Basic Science, Project Code IBS-R024-D1. SF thanks Konstantin Kladko for discussions during a visit to IBS, which led to the main idea of machine learning based chaos testing, and Natalia Khotkevych for early attempts to figure a realization pathway.

### Data availability

The data that support the findings of this study are available upon reasonable request from the authors.

1  
2      *Deep Learning of Chaos Classification*  
3  
4  
5  
6

13

7      **Appendix A. Details of the neural network structure**  
8  
9  
10  
11  
12  
13  
14  
15  
16  
17  
18  
19

The neural network model we use to analyze the chaotic pattern is the convolutional neural network (CNN) [14] with a fully connected (FC) network [16, 17]. The required nonlinear response of the system is provided by the rectified linear unit (ReLU) [17, 18]. For supervised learning, we use a cross entropy as loss function [17]. Fig. A1 shows one of the CNN structures used here. In the figure, 1024 filters in the first layer scan the input data independently, then yield 1024 feature maps which are used as the input data for the second layer after applying the activation function ReLU. After processing through all convolutional layers, we rearranged the pixels of the last feature maps into one-dimensional data for the fully connected layers. In the last layer we set the desired output: 1 is a chaotic, and 0 is a regular trajectory.

We use a two-dimensional convolutional filter. The data comprise multiple spatial channels and each channel gives time-series data. The relation between the 2D input vector  $a$  and the convolution layer output vector  $z$  is

$$z_{i,j,m}^{(\ell)} = \sum_{q=1}^{F_{row}} \sum_{p=1}^{F_{col}} w_{p,q,m}^{(\ell)} a_{(i+p-1),(j+q-1)}^{(\ell-1)} + b_m^{(1)}. \quad (\text{A.1})$$

After calculating  $z$ , the nonlinear activation function (We used ReLU) is used to obtain the value of  $a$  of the next layer:

$$a_{i,j,m}^{(\ell)} = \text{ReLU}(z_{i,j,m}^{(\ell)}), \quad (\text{A.2})$$

where  $i, j$  are input element indices,  $p, q$  are filter element indices,  $m$  is the filter index (e.g.  $m = 1024$  means that 1024 filters of size  $F_{row} \times F_{col}$  were used), and  $\ell$  is the layer index (the indices of input and first layer are  $\ell = 0$  and  $\ell = 1$  respectively). The weight  $w_{p,q,m}^{(\ell)}$  is the  $(p, q)^{th}$  element of  $m^{th}$  filter. The bias  $b_m$  is a constant. The filter size is  $F_{row} \times F_{col}$ , where we chose  $F_{row} = 2$  and  $F_{col} = 1$ . To apply the filter to all the elements of the input, the boundary is filled with zeroes to match the size of the input, which is called zero padding [19]. The 2D input through the convolution layer has a dimension of  $(i, j, m)$  due to the number of filters  $m$  in the convolution layer. Accordingly, the input / output relationship of the next layer is as follows:

$$z_{i,j,n}^{(\ell)} = \sum_{n=1}^{M_\ell} \sum_{q=1}^{F_{row}} \sum_{p=1}^{F_{col}} w_{p,q,n}^{(\ell)} a_{(i+p-1),(j+q-1),m}^{(\ell-1)} + b_n^{(\ell)}, \quad (\text{A.3})$$

where  $M_\ell$  is the number of filters between the  $\ell^{th}$  and  $(\ell - 1)^{th}$  layers,  $\ell$  has a range of 1 to  $L$ . After convolution, it processes through the activation function as shown in Eq. A.2.

As shown in Fig. A1, there is a pooling layer at the end of the convolution layers. This flattens the convolutional output by finding the maximum according to the filter dimension of the input (Eq. A.4).

1  
2     *Deep Learning of Chaos Classification*  
3  
4  
5

14

$$a_m^{(\ell)} = \max(a_{i,j,m}^{(\ell)}). \quad (\text{A.4})$$

8     The reason for flattening the output is to use the convolutional output as the input of  
9     the fully connected layer:  
10

$$z_i^{(\ell)} = \sum_{j=1}^K w_{j,i}^{(\ell-1)} a_j^{(\ell-1)}, \quad (\text{A.5})$$

15     where  $w_{i,j}$  is a weighted connection between the  $j^{th}$  component of  $(\ell-1)^{th}$  layer and  
16     the  $i^{th}$  component of  $(\ell)^{th}$  layer and  $K$  is the number of nodes in the  $(\ell-1)^{th}$  layer. As  
17     in Eq. A.6, the activation function uses ReLU:  
18

$$a_i^{(\ell)} = \text{ReLU}(z_i^{(\ell)}). \quad (\text{A.6})$$

22     The output value of the network, when obtained in this way, is different from the  
23     desired output because it is obtained from the unfitted  $w$  value.  $w$  updates in the  
24     direction of reducing this difference and we call this difference the loss or cost. In this  
25     work, we selected the cross entropy as the loss function, defined as  
26

$$C = - \sum_{k=1}^{N_L} (a_k^{true} \log(a_k^{(L)}) + (1 - a_k^{true}) \log(1 - a_k^{(L)})), \quad (\text{A.7})$$

32     where  $N_L$  is the number of nodes in the output layer and  $a_k^{true}$  is the desired output at the  
33      $k^{th}$  node. The cross-entropy loss function can reflect the degree of error to weight updates  
34     better than the mean square error loss function (MSE,  $\text{MSE} = \frac{1}{N_L} \sum_{k=1}^{N_L} (a_k^{true} - a_k^{(L)})^2$ )  
35     because of the log term and is known as a cost function suitable for classification  
36     problems [20]. Similar to the energy minimization problem in physics, supervised  
37     learning minimizes a cost function  $C$  at the output layer.  
38

40     Training the neural network means finding optimized parameters  $w_{pqm}^{(\ell)}$  and  $b_n^{(l)}$   
41     that minimize  $C$ . We use an Adaptive Moment Estimation (Adam) algorithm for the  
42     optimization of learning [21]. As far as we know, the choice of optimization algorithm  
43     has little impact on the network performance, but is instead mainly related to the speed  
44     of learning. It is known that an Adam algorithm can find fitting variables faster than  
45     stochastic gradient descent methods, RMSprop and AdaDelta [21].  
46

49     **Appendix B. Network comparison**  
50

52     In this section, we compare three different network architectures. First, we consider a  
53     fully connected neural network (FCN) and then compare it to other machine learning  
54     methods. The FCN is chosen because it is the most basic structure of deep learning  
55     classifiers. We also consider a recurrent neural network (RNN) [22]. The RNNs  
56     are usually used to deal with temporal dynamic behavior. We consider supervised  
57     classification with labels indicating chaos or regularity, where the input of the neural  
58     59

60

## Deep Learning of Chaos Classification

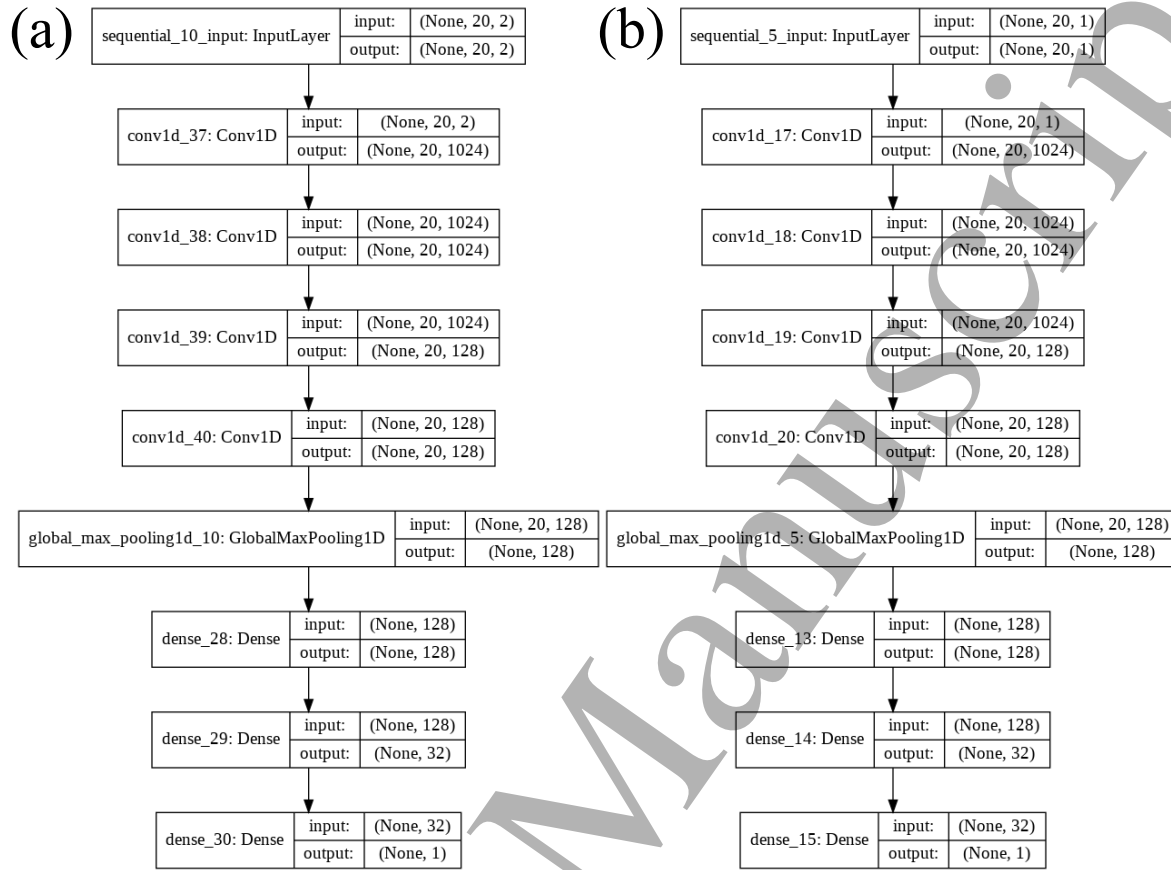


**Figure A1.** Network architecture for chaos classification, consisting of four convolution layers, and three fully-connected layers. The filter size and output size are provided for each layer. Network structure for (a) 2D and (b) 1D shape training.

networks is fixed at  $N_K = 20$ , and the output is one node for the corresponding label for training. The neural networks presented in this paper end with a sigmoid layer.

The first type of network considered in this section is a fully connected network, which consists of multiple fully connected layers and each layer has a nonlinear activation function. We use eight hidden layers with ReLU (Rectified Linear Unit) activation and the number of hidden neurons in each layer is [256, 256, 512, 512, 512, 256, 128, 64]. The network is trained with the Adaptive Moment Estimation (Adam) algorithm [21].

Recurrent neural networks (RNN) are neural networks for processing sequential data. RNN uses the current input as well as any previously processed input. This is possible with a loop structure between the RNN input and the output. Each node in a given layer is connected with a directed connection to the current layer. Because of this, the RNN is expected to have a function of memory. The sequence itself has information, and recurrent networks use this information through the loop structure. We use three type of RNNs: simpleRNN [22], LSTM [22,23], and GRU [24]. Three RNN cells(layers) were used, each with 200 hidden neurons. After the RNN cells, three fully connected layers are connected with the size of 200, 100 and 32 respectively. It is known that

1  
2     *Deep Learning of Chaos Classification*  
3  
4  
5  
6  
7

recurrent networks perform well for sequential data, but at least in our data sets there was no significant difference between using CNN and RNN.

Classifiers	$P_{tot}$	$P_C$	$P_R$
FCN	0.89	0.88	0.91
SimpleRNN	0.94	0.96	0.92
GRU	0.95	0.96	0.93
LSTM	0.94	0.96	0.93
CNN	0.96	0.94	0.97

**Table B1.** Performance for different deep learning classifiers. The networks are trained with chaotic and regular trajectories for  $K_{min} = 1.0$ ,  $K_{max} = 2.0$ ,  $M_K = 11$ ,  $M_{tr} = 2601$  and  $N_K = 20$ . The network performances are evaluated for  $K_{min} = 3.0$ ,  $K_{max} = 3.5$ ,  $M_K = 6$ ,  $M_{tr} = 2601$  and  $N_K = 20$ . For each K value, 2601 different initial values  $(p_{0,i}, x_{0,j})$  were selected as  $(p_{0,i} = (i-1)\frac{1}{50}, x_{0,j} = (j-1)\frac{1}{50}, (i, j \in \mathbb{Z}, 1 \leq i, j \leq 51, ))$ .

24  
25  
26     **References**  
27  
28

- [1] James E Skinner, Ary L Goldberger, Gottfried Mayer-Kress, and Raymond E Ideker. Chaos in the heart: implications for clinical cardiology. *Nature Biotechnology*, 8(11):1018–1024, 1990.
- [2] Julia Slingo and Tim Palmer. Uncertainty in weather and climate prediction. *Philosophical Transactions of the Royal Society A: Mathematical, Physical and Engineering Sciences*, 369(1956):4751–4767, 2011.
- [3] Edward Ott. *Chaos in Dynamical Systems*. Cambridge University Press, Cambridge, 2 edition, 2002.
- [4] Samuel Dodge and Lina Karam. A study and comparison of human and deep learning recognition performance under visual distortions. In *2017 26th international conference on computer communication and networks (ICCCN)*, pages 1–7, United States, 2017. Institute of Electrical and Electronics Engineers Inc.
- [5] Ahmed Ali Mohammed Al-Saffar, Hai Tao, and Mohammed Ahmed Talab. Review of deep convolution neural network in image classification. In *2017 International Conference on Radar, Antenna, Microwave, Electronics, and Telecommunications (ICRAMET)*, pages 26–31, United States, 2017. Institute of Electrical and Electronics Engineers Inc.
- [6] Samuel H. Rudy, Steven L. Brunton, Joshua L. Proctor, and J. Nathan Kutz. Data-driven discovery of partial differential equations. *Science Advances*, 3(4), 2017.
- [7] Jiequn Han, Arnulf Jentzen, and Weinan E. Solving high-dimensional partial differential equations using deep learning. *Proceedings of the National Academy of Sciences*, 115(34):8505–8510, 2018.
- [8] Maziar Raissi and George Em Karniadakis. Hidden physics models: Machine learning of nonlinear partial differential equations. *Journal of Computational Physics*, 357:125 – 141, 2018.
- [9] Shreya Agrawal, Luke Barrington, Carla Bromberg, John Burge, Cenk Gazen, and Jason Hickey. Machine learning for precipitation nowcasting from radar images. *arXiv preprint arXiv:1912.12132*, 2019.
- [10] Jaideep Pathak, Brian Hunt, Michelle Girvan, Zhixin Lu, and Edward Ott. Model-free prediction of large spatiotemporally chaotic systems from data: A reservoir computing approach. *Phys. Rev. Lett.*, 120:024102, Jan 2018.
- [11] Allan J Lichtenberg and Michael A Lieberman. *Regular and chaotic dynamics*, volume 38. Springer, New York, 2013.

1  
2     *Deep Learning of Chaos Classification*  
3  
4

17

- 5 [12] Mirella Harsoula, Kostas Karamanos, and George Contopoulos. Characteristic times in the  
6 standard map. *Phys. Rev. E*, 99:032203, Mar 2019.
- 7 [13] Bharath Ramsundar and Reza Bosagh Zadeh. *TensorFlow for deep learning: from linear regression*  
8 *to reinforcement learning*. O'Reilly Media, Sebastopol, 2018.
- 9 [14] Yann LeCun, Patrick Haffner, Léon Bottou, and Yoshua Bengio. *Object Recognition with Gradient-*  
10 *Based Learning*, pages 319–345. Springer Berlin Heidelberg, Berlin, Heidelberg, 1999.
- 11 [15] George M Zaslavsky. *Physics of Chaos in Hamiltonian Systems*. Imperial College Press, London,  
12 1998.
- 13 [16] Alex Krizhevsky, Ilya Sutskever, and Geoffrey E Hinton. Imagenet classification with deep  
14 convolutional neural networks. In F. Pereira, C. J. C. Burges, L. Bottou, and K. Q. Weinberger,  
15 editors, *Advances in Neural Information Processing Systems 25*, pages 1097–1105. Curran  
16 Associates, Inc., 2012.
- 17 [17] Ian Goodfellow, Yoshua Bengio, and Aaron Courville. *Deep Learning*. Adaptive Computation  
18 and Machine Learning series. MIT Press, Cambridge, 2016.
- 19 [18] Vinod Nair and Geoffrey E Hinton. Rectified linear units improve restricted boltzmann machines.  
20 In *Proceedings of the 27th international conference on machine learning (ICML-10)*, pages 807–  
21 814, Madison, 2010. Omnipress.
- 22 [19] Vincent Dumoulin and Francesco Visin. A guide to convolution arithmetic for deep learning.  
23 *arXiv preprint arXiv:1603.07285*, 2016.
- 24 [20] Michael A Nielsen. *Neural Networks and Deep Learning*. Determination Press, San Francisco,  
25 2015.
- 26 [21] Diederik P. Kingma and Jimmy Ba. Adam: A method for stochastic optimization. In Yoshua  
27 Bengio and Yann LeCun, editors, *3rd International Conference on Learning Representations,*  
28 *ICLR 2015, San Diego, CA, USA, May 7-9, 2015, Conference Track Proceedings*, 2015.
- 29 [22] Alex Sherstinsky. Fundamentals of recurrent neural network (rnn) and long short-term memory  
30 (lstm) network. *Physica D: Nonlinear Phenomena*, 404:132306, 2020.
- 31 [23] Felix A. Gers, Jürgen Schmidhuber, and Fred Cummins. Learning to forget: Continual prediction  
32 with lstm. *Neural Computation*, 12:2451–2471, 1999.
- 33 [24] Kyunghyun Cho, Bart van Merriënboer, Caglar Gulcehre, Dzmitry Bahdanau, Fethi Bougares,  
34 Holger Schwenk, and Yoshua Bengio. Learning phrase representations using RNN encoder–  
35 decoder for statistical machine translation. In *Proceedings of the 2014 Conference on Empirical*  
36 *Methods in Natural Language Processing (EMNLP)*, pages 1724–1734, Doha, October 2014.  
37 Association for Computational Linguistics.
- 38
- 39
- 40
- 41
- 42
- 43
- 44
- 45
- 46
- 47
- 48
- 49
- 50
- 51
- 52
- 53
- 54
- 55
- 56
- 57
- 58
- 59
- 60